ACCOUNTING FOR FIBER COLLISIONS IN THE GALAXY POWER SPECTRUM MEASUREMENTS

ChangHoon Hahn[1], Roman Scoccimarro[1], Michael R. Blanton[1], moreauthors
Draft version December 16, 2015

ABSTRACT

Fiber-fed multi-object spectroscopic surveys, with their ability to collect an unprecedented number of redshifts, dominate cosmological studies. However physical constraints, which limit these surveys from successfully collecting redshifts from galaxies too close to each other on the focal plane, ultimately lead to significant systematic effects on galaxy clustering measurements. Using simulated mock catalogs, extensively used in interpreting large-scale structure clustering results of the Sloan Digital Sky Survey, we investigate the effects of fiber collisions on the galaxy power spectrum monopole and quadrupole and compare methods currently used to correct for fiber collisions in the literature and assess their success in reconstructing the true power spectrum.

We present two methods to account for fiber collisions in the power spectrum. The first method statistically reconstructs the clustering of fiber collided galaxy pairs by modeling the distribution of the line-of-sight displacements between them using cases where both redshifts are obtained. The method properly accounts for fiber collisions in the shot-noise correction term of the power spectrum estimator. For the monopole, this method reproduces the true power spectrum for the mock catalogs with residuals of $< 1\%$ at $k \sim 0.3 \ h/\mathrm{Mpc}$ and $< 10\%$ at $k \sim 0.8 \ h/\mathrm{Mpc}$ – a significant improvement from existing correction methods, especially at small scales ($k > 0.1 \ h/\mathrm{Mpc}$). In our second method, we model the effect of fiber collisions on the true galaxy power spectrum by Fourier transforming an analytical estimate of the effect of fiber collisions on the two-point correlation function. Using this method we are able to reproduce the power spectrum quadrupole with fiber collisions from the true power spectrum to within sample variance for $k < 0.6 \ h/\mathrm{Mpc}$ (**MADEUPNUMBER**). **INCLUDE MORE NUMBERS**. With statistical uncertainty no longer dominating galaxy clustering measurements, the methods we present in accounting for fiber collisions will allow us to extend power spectrum measurements to smaller scales than previous possible.

Subject headings: cosmology: observations – cosmology: large-scale structure of universe – galaxies: distances and redshift – galaxies: halos – galaxies: statistics

1. INTRODUCTION

As of 2015, millions of redshifts to distance galaxies have been obtained through redshift surveys. Cosmological measurements such as galaxy clustering statistics are no longer dominated by uncertainties from statistical precision, but from systematic effects of the measurements. These surveys, such as the 2dF Galaxy Redshift Survey (2dFGRS; Colless 1999) and the Sloan Digital Sky Survey III Baryon Oscillation Spectroscopic Survey (SDSS-III BOSS; Anderson et al. 2012; Dawson et al. 2013) and future surveys such as the Extended Baryon Oscillation Spectroscopic Survey (eBOSS; Dawson et al. 2015), use fiber-fed spectrographs.

For each galaxy, a fiber is used to obtain a spectroscopic redshift. However, due to the physical size of the fiber housing, if two galaxies are located within the fiber collision angular scale from one another on the sky, separate fibers cannot be placed adjacently to observe them simultaneously (Yoon et al. 2008 **CITE MORE?**). In these situations, the redshifts of only a single redshift is measured. With redshifts of galaxies in close angular proximities missing from the sample, any clustering statistic probing these scales will be systematically affected.

As our cosmological surveys extend further to higher redshifts, the systematic effect becomes more severe, because the fiber collision angular scale corresponds to a larger comoving scale, thereby affecting our measurements on larger scales. SDSS-III BOSS, in particular, has an angular fiber collision scale of $62''$. This corresponds to $\sim 0.43 \ \mathrm{Mpc}/h$ at the center of the survey's redshift redshift range; fiber-collided galaxies account for $\sim 5\%$ of the galaxy sample (Anderson et al. 2012). While this may seem like a relatively small fraction of redshifts, its effect on clustering measurements such as the power spectrum is significant and need be accounted for in order to probe smaller scales and higher order statistics such as the three-point correlation function or the bispectrum. Future spectroscopic surveys such as the Dark Energy Survey Instrument (DESI; Schlegel et al. 2011; Morales et al. 2012; Makarem et al. 2014), will use robotic fiber positioner technology. Unfortunately this will only increase the effect of fiber collisions. Therefore, accounting for fiber collisions will be an unavoidable challenge for clustering statistics in the near future.

To correct for fiber collisions, one common approach used in clustering statistics is the nearest neighbor method (Zehavi et al. 2002; Berlind et al. 2006; Anderson et al. 2012). For fiber-collided galaxies without resolved redshifts, the method assigns the statistical weight of the fiber-collided galaxy to its nearest angular neighbor. This provides a reasonable correction for the fiber collision effects at scales much larger than the fiber col-

[1] Center for Cosmology and Particle Physics, Department of Physics, New York University, 4 Washington Place, New York, NY 10003; chh327@nyu.edu

lision scales; however the correction falls short near the fiber collision scale. In fact, as Zehavi et al. (2005) find, fiber collisions affect the two-point correlation function (2PCF) measurements even on scales significantly larger than the fiber collision scale (> 1 Mpc/h). For power spectrum measurements in BOSS, the nearest neighbor method has often been supplemented with adjustments in the constant shot-noise term of the power spectrum estimator to correct for fiber collisions (Beutler et al. 2014; Gil-Marín et al. 2014). While this shot-noise term adjustment has been calibrated within the mock catalogs used to interpret the BOSS clustering results there is no way to validate and calibrate these methods independently for observations. Methods of this kind rely entirely on the accuracy of the mock catalogs to constrain fiber collisions, which is especially concerning since fiber collisions systematically affect small scales and mock catalogs may not be reliable at such small scales (Heitmann et al. 2008; Schneider et al. 2015).

Recently Guo et al. (2012), focusing on SDSS-III BOSS like samples, proposed a fiber collision correction method for the 2PCF that is able to reasonably correct for fiber collisions above and below the collision scale. Guo et al. (2012) estimates the total contribution of fiber-collided galaxies to the two point correlation function by examining the pair statistics in overlapping tiling regions of the survey, where a smaller fraction of galaxies suffer from fiber collisions. Unfortunately, applying this method to Fourier clustering measurements is intractable due to the complex geometry of the overlapping regions. As a result, we propose two methods to account for fiber collisions in power spectrum measurements. The first improves upon the nearest neighbor method by using the distribution of the line-of-sight displacement between resolved fiber collided galaxies to statistically reconstruct the clustering of fiber-collided galaxies; and properly accounts for fiber collisions in the shot-noise correction term of the power spectrum estimator. This method seeks to recover the true power spectrum from fiber collided galaxy catalogs. The second, on the other hand, uses the Fourier transform of an analytic estimate of the effect of fiber collisions in the 2PCF in order to model the effect of fiber collisions and reproduce the fiber collided power spectrum from the true power spectrum.

In Section 2, we briefly describe the simulated mock catalogs with realistically applied fiber collisions and the power spectrum estimator used throughout the paper. We demonstrate the effects of fiber collisions on power spectrum measurements and how the nearest neighbor method does not adequately account for fiber collisions at small scales in Section 3.1. We then present our two methods of accounting for fiber collisions in Section 3.2 and Section **??** respectively. We then apply our methods to the mock catalogs and compare correction methods in the literature in Section 4. Finally in Section 5 we summarize and discuss our results.

2. FIBER-COLLIDED MOCK CATALOGS

For various purposes such as calculating covariance matrices or estimating cosmic variance, simulated mock catalogs play a crucial role in interpreting clustering measurements of observed galaxies (Scoccimarro & Sheth 2002; Anderson et al. 2012; Manera et al. 2013). They also provide a means of understanding systematic effects
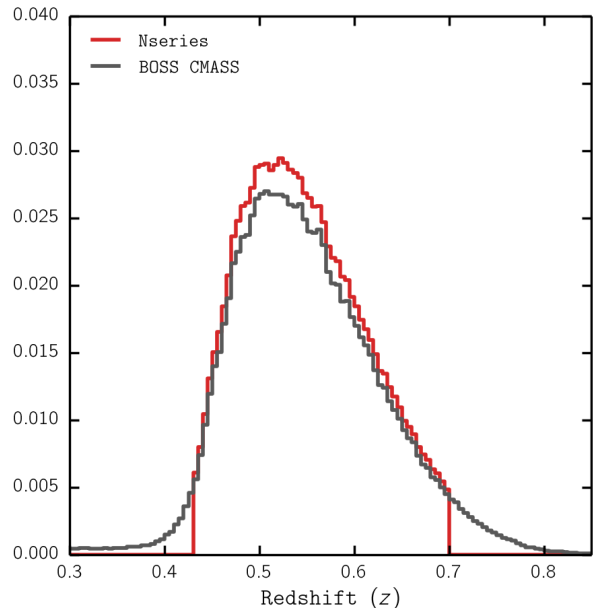

Fig. 1.— Normalized galaxy redshift distribution for LasDamas (blue), QPM (orange), and Tiling Mock (green) mock catalogs. The normalized redshift distribution of BOSS DR12 CMASS is also plotted (black). Bin size of $\Delta z = 0.025$ was used to compute the each of the distributions. LasDamas mock catalog has a constant number density of galaxies throughout $0.16 < z < 0.44$, the redshift range of SDSS LRG sample. QPM and Tiling Mock catalogs, on the other hand, trace the BOSS CMASS redshift distribution ($0.43 < z < 0.7$).

such as fiber collisions (Guo et al. 2012; Manera et al. 2013 **LIST MORE**) since systematic effects can be simulated on the mock catalogs. This allows us to test how these effects influence clustering measurements and devise correction methods that attempt to account for these effects.

A direct way of understanding the effects of fiber collisions on clustering statistics in observations is to first apply fiber collisions to mock catalogs and then compare the clustering statistics obtained from mock catalogs with and without the fiber collisions. Correction methods for fiber collisions can then be applied to the fiber-collided mocks and the merit of the correction method can be quantified by how successfully they reproduce the clustering statistics of the original mock catalogs without fiber collisions. The optimal correction method can then be applied to the observed data with some assurance that it accounts for fiber collisions and improves the clustering measurements.

When applying the fiber collisions to the mock catalogs, it is essential to apply them in the same manner they affect the observational data. For BOSS, galaxies within $62''$ are fiber-collided (Anderson et al. 2012). In reality, this simple criteria is further complicated by the tiling scheme of observing plates that create overlapping regions, which have a higher success rate in resolving galaxy spectra within the fiber collision angular scale (Guo et al. 2012). Furthermore, fiber collisions are only one of the systematic effects that influence BOSS data. Systematic effects include the unique geometry of the BOSS survey, the variable completeness in different sectors of the survey, and redshift failures (Anderson et al. 2012).

Effects of fiber collisions must be understood and interpreted in conjunction with these other systematic effects. Therefore, in this paper, we use LasDamas (McBride et al. 2009, 2011), Quick Particle Mesh (White et al. 2014), and Nseries (**CITATION?**) catalogs, which have already been extensively used in interpreting clustering results for SDSS and BOSS and are generated through different prescriptions. Therefore they provide a robust sets of data to measure the effects of fiber collisions and to test our correction method tailored for BOSS.

The LasDamas Galaxy mock catalogs is constructed from the Oriana N-body Large Suite of Dark Matter Simulations (LasDamas) with 1280^3 particles with a box with side length, $L_{\mathrm{Box}} = 2400$ Mpc/h. The N-body LasDamas simulations uses a spatially flat ΛCDM cosmology with $\Omega_{\mathrm{m}} = 0.25$, $\Omega_{\Lambda} = 0.75$, $\Omega_{\mathrm{b}} = 0.04$, $\sigma_8 = 0.8$, $n_{\mathrm{s}} = 1$ and $h = 0.7$. The dark matter halos are then identified using a friends-of-friends (FOF) algorithm (Davis et al. 1985) with a linking length $b = 0.2$ times the mean interparticle separation. The over-densities of dark matter halos are then populated with galaxies using the halo occupation distribution (HOD) framework to construct the galaxy mock catalogs (McBride et al. 2009, 2011). The HOD prescription is specified so that the galaxy mock catalogs reproduce the galaxy number density and projected correlation function of the observed SDSS Luminous Red Galaxy sample with $M_g < -21.8$. The LasDamas galaxy mock catalogs have 40 realizations each of which spans the redshift range, $0.16 < z < 0.44$ and are restricted to the survey geometry of SDSS Data Release 7. They also include redshift space distortions from velocities, but do not model fiber collisions.

To model the fiber collisions of the observed galaxies in BOSS, we impose fiber collisions at the angular scale of $62''$. Once we identify galaxies within $62''$ of each other, we arbitrary select one of the galaxies and assign the statistical weights of the other galaxies within $62''$ of it. Roughly $\sim 2.5\%$ of the galaxies in the LasDamas mock catalogs are affected by fiber collisions.

Next, the QPM mock galaxy catalogs uses a "quick particle mesh" method, which uses a low resolution particle-mesh N-body solver to evolve particles within a period simulation volume. The particles are assigned halo masses in order to match the halo mass function and large-scale bias of halos of high resolution simulations. Afterward the Tinker et al. (2012) HOD parameterization is used to populate the halos. The mock galaxy sample is then trimmed to the BOSS CMASS survey footprint, downsampled based on angular sky completeness (sector completeness) and radial selection. Furthermore, QPM mocks model the fiber collisions of the BOSS CMASS sample ($62''$ angular fiber collision scale). The QPM galaxy mock catalog uses the following ΛCDM cosmology: $\Omega_{\mathrm{m}} = 0.29$, $\Omega_{\Lambda} = 0.71$, $\sigma_8 = 0.8$, $n_{\mathrm{s}} = 0.97$ and $h = 0.7$. We use 1000 realizations of the QPM galaxy mock catalog. For a detailed description of the QPM galaxy mock catalogs we refer readers to White et al. (2014).

Finally the Tiling Mock catalog is generated using **INSERT TILING MOCK DESCRIPTION HERE**

In Figure 2, we plot the redshift distribution for LasDamas, QPM, and Tiling Mock catalogs along with the redshift distribution of BOSS DR12 galaxies. The Las-

Damas mock catalog, which is constructed based on the SDSS LRG sample has a constant $\bar{n}(z)$ over the redshift $0.16 < z < 0.44$, while the QPM and Tiling mock redshift distributions closely trace the observed BOSS redshift distribution (roughly $0.43 < z < 0.7$).

2.1. *Power Spectrum Estimator*

In this paper, we focus on the effects of fiber collisions on the galaxy power spectrum out of the other clustering measurements, more specifically the monopole and quadrupole of the power spectrum. Throughout the paper, when we measure the power spectrum we use the estimator described in Scoccimarro (2015) and the formalism therein. To reiterate Section III. A. in Scoccimarro (2015), we calculate the monopole component of the power spectrum using:

$$\widehat{P_0}(k) = \frac{1}{I_{22}} \left[\int \frac{d\Omega_k}{4\pi} |F_0(\mathbf{k})|^2 - N_0 \right] \quad (1)$$

where

$$F_0(\mathbf{k}) = \left(\sum_{j=1}^{N_g} - \alpha \sum_{j=1}^{N_r} \right) w_j \; e^{i\mathbf{k}\cdot\mathbf{x}_j} \quad (2)$$

with standard normalization constant

$$I_{22} = \alpha \sum_{j=1}^{N_g} \bar{n}(\mathbf{x}_j) w_j^2 \quad (3)$$

and shot noise term

$$N_0 = \left(\sum_{j=1}^{N_g} - \alpha^2 \sum_{j=1}^{N_r} \right) w_j^2. \quad (4)$$

N_0 represents the constant shot noise contribution to the power due to the discrete density field of our galaxies. α is the ratio of the number of galaxies (N_g) over the number of synthetic random galaxies (N_r), $\bar{n}(\mathbf{x})$ is the mean density of the galaxies at position $\mathbf{x}$, and w_j is weight of each object, which includes the the minimum variance weight derived in Feldman et al. (1994):

$$w_{\mathrm{FKP}}(\mathbf{x}_j) = \frac{1}{1 + \bar{n}(\mathbf{x}_j) P_0} \quad (5)$$

where P_0 is the power spectrum amplitude at which the error is minimized. We use $P_0 = 20000$ Mpc^3/h^3 for our analysis, which corresponds to $k \sim 0.1$ h/Mpc. We note that the shot noise term in Eq. 4 differs from the standard shot noise term from Feldman et al. (1994), which uses $N_0^{\mathrm{FKP}} = \alpha(1+\alpha) \sum_{j=1}^{N_r} w_j^2$. The difference between shot noise formulations will be discussed further in Section 3.3.

For the quadrupole,

$$\widehat{P_2}(k) = \frac{5}{I_{22}} \int \frac{d\Omega_k}{4\pi} F_2(\mathbf{k}) F_0^*(\mathbf{k}) \quad (6)$$

where

$$F_2(\mathbf{k}) = \frac{3}{2} \hat{k}_a \hat{k}_b Q^{ab}(\mathbf{k}) - \frac{1}{2} F_0(\mathbf{k}) \quad (7)$$
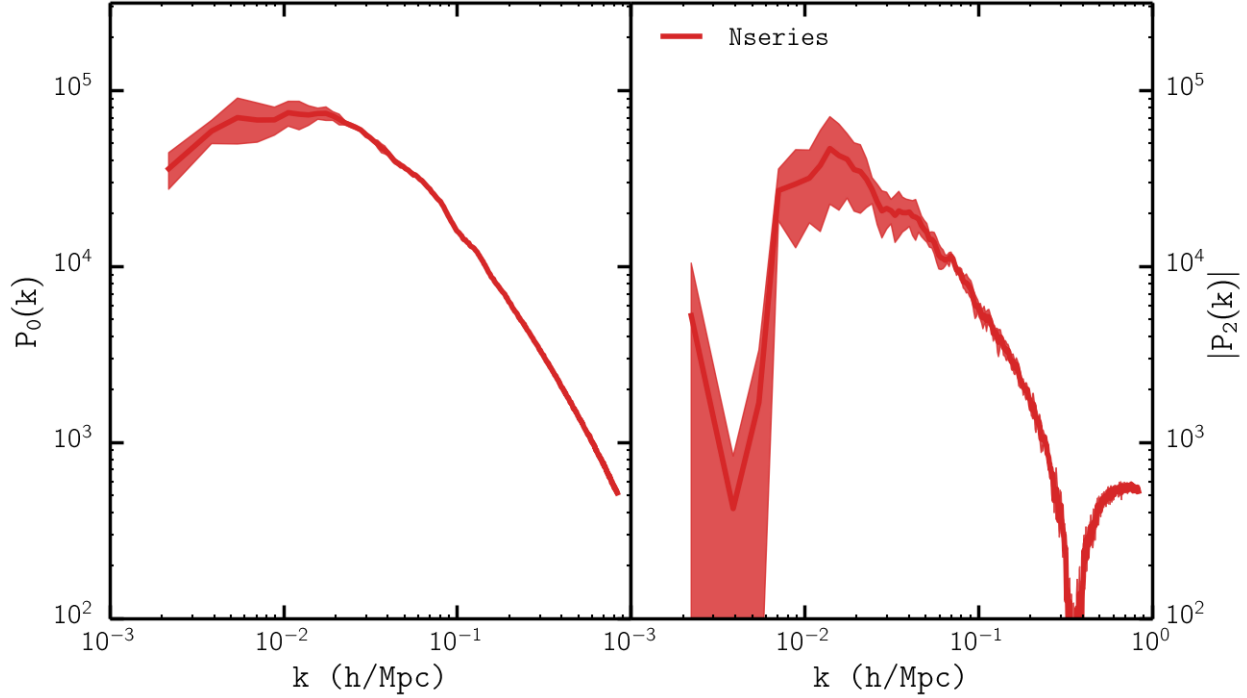
FIG. 2.— Average power spectrum monopole $\overline{P_0(k)}$ and quadrupole $|\overline{P_2(k)}|$ for BOSS DR12 (black) and the mock catalogs LasDamas (blue), QPM (orange), Nseries (red), and Tiling Mock (green), listed in Section 2 using the estimator from Scoccimarro (2015). The width of the $P_l(k)$ for LasDamas and QPM represent the sample variance ($\Delta P_l(k)$) calculated from the realizations of the mock catalogs. For $l = 2$, we plot the absolute value of $P_2(k)$ because $P_2(k) < 0$ for $k \gtrsim 0.35\ h/\text{Mpc}$. We emphasize that fiber collisions were not applied to the mock catalogs for the measurements above. Meanwhile, galaxy weights (Equation 9) are applied to the BOSS DR12 $P_l(k)$ measurements. We remind readers that the LasDamas mock catalog has an overall greater $\overline{P(k)}$ due to the fact that the catalog spans the SDSS LRG sample redshift range instead of the BOSS redshift range of the other mock catalogs.

with

$$Q^{ab}(\mathbf{k}) = \left(\sum_{j=1}^{N_g} -\alpha \sum_{j=1}^{N_r}\right) \hat{x}_j^a \hat{x}_j^b w_j\, e^{i\mathbf{k}\cdot\mathbf{x}_j} \qquad (8)$$

In Figure 2, we plot the $P_0(k)$ and $P_2(k)$ calculated using Eq. 1 and Eq. 6, respectively, for LasDamas, QPM, and Tiling mock catalogs. The fiber collisions described previously are not applied to the mock catalogs in the $P(k)$ calculations. Without fiber collisions, the weights of the objects is equivalent to the FKP weights, $w_j = w_{j,\text{FKP}}$.

We also plot the $P_0(k)$ and $P_2(k)$ from the BOSS Data Release 12 CMASS data (black) in Figure 2. For BOSS DR12 CMASS, systematic weights are assigned to the galaxies in order to account for sector completeness, redshift failures, and fiber collisions. Each galaxy has a statistical weight determined by,

$$w_{j,\text{tot}} = w_{j,\text{sys}}(w_{j,\text{rf}} + w_{j,\text{fc}} - 1), \qquad (9)$$

(Anderson et al. 2012; Beutler et al. 2014), which are included in the object weights w_j along with $w_{j,\text{FKP}}$. The statistical weights are also included in the factor α. So for the BOSS $P_0(k)$ and $P_2(k)$ calculations, $w_j = w_{j,\text{tot}} \times w_{j,\text{FKP}}$ and $\alpha' = \sum_{j=1}^{N_g} w_{\text{tot}}/N_r$.

Furthermore, for the mock catalogs with multiple realizations (LasDamas, QPM and Nseries), we compute the sample variance of the power spectrum monopole and quadrupole

$$\Delta P_l(k) = \sqrt{\frac{1}{N_{\text{mocks}}} \sum_{i=1}^{N_{\text{mocks}}} (P_l^i(k) - \overline{P_l(k)})^2}\ \ (l = 0, 2).$$

$$(10)$$

N_{mock} is the total number of realizations (40 for LasDamas and 1000 for QPM) and $P_l^i(k)$ is the power spectrum ($l = 0$ monopole, $l = 2$ quadrupole) for each realization. $\Delta P(k)$ is represented by the width of the $P(k)$ in Figure 2.

3. FIBER COLLISION METHODS

3.1. Nearest Angular Neighbor Method

A common approach in accounting for fiber collisions in clustering measurements has been to use the nearest angular neighbor method (Zehavi et al. 2002; Berlind et al. 2006; Anderson et al. 2012), hereafter NN method. For galaxies without resolved spectroscopic redshifts due to fiber collisions, the entire statistical weight of the galaxy is assigned to its nearest angular neighbor. This method effectively assumes that all galaxies within the angular fiber collision scale ($< 62''$ for BOSS) are correlated with one another. In other words, the method assumes that galaxies within the fiber collision angular scale reside in the same halo so displacing one of the galaxies and placing it on top of the other does not significantly alter the clustering statistics. One consequence of this method however is that galaxies within the angular fiber collision scale purely by coincidence (hereafter referred to as
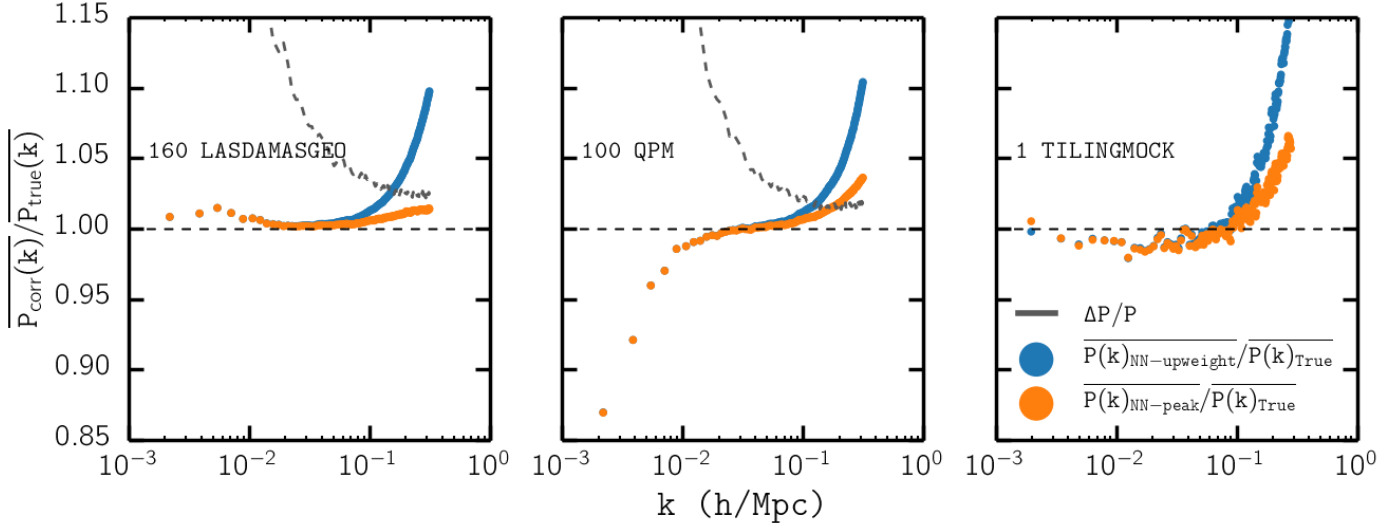
FIG. 3.— The ratio of $\overline{P_{\rm corr}(k)}$ using the nearest-neighbor (NN) correction (blue) and $d_{\rm LOS}$-peak correction (orange) over the true $\overline{P(k)}$ for LasDamas (left panel), QPM (middle panel), and Tiling Mock (right panel) catalogs. The NN correction and $d_{\rm LOS}$-peak correction methods are described in Section 3.2.1. We also plot the ratio of the sample variance to the true $\overline{P_{\rm true}(k)}$, $\Delta P_{\rm true}(k)/\overline{P_{\rm true}(k)}$ (black; dashed) for comparison. Incorporating the $d_{\rm LOS}$ distribution significantly improves the correction of fiber collisions for $k > 0.1\ h/{\rm Mpc}$; however, neither method is able to constrain the systematic effects of fiber collisions significantly below the sample variance at $k > 0.2\ h/{\rm Mpc}$.

"chance alignments") are incorrectly assumed to be grav- itationally correlated, so when their statistical weight is added to its nearest angular neighbor, they are in fact displaced significantly from their true position. For BOSS, the nearest angular neighbor method can displace galaxies by up to 500 Mpc. Furthermore even for fiber- collided galaxies that reside in the same group or cluster, up-weighting the nearest neighbor ignores halo-scale line- of-sight displacements.

To precisely quantify the effect of fiber collisions on the power spectrum, in Figure 3, we compare $P_0(k)$ and $P_2(k)$ measured using the NN method for mock catalogs with fiber collisions to the $P_0(k)$ and $P_2(k)$ measure- ments for mock catalogs without fiber collisions. The $P_0(k)$ measurements are made using Eq. 1 with a stan- dard FKP shot noise (N_0^{FKP}) rather than N_0 from Eq. 4, which is effectively just the standard power spectrum estimator from Feldman et al. (1994). $P_2(k)$ measure- ments are made using Eq. 6. **Description of Figure 3 focusing on the scales where the NN method breaks down and quantifying the residuals.**

In order to correct for this effect, in following section we present an improved method to account for correlated fiber collided galaxies that uses the line-of-sight displace- ment between fiber collided pairs (Section 3.2.1) and a corrected shot-noise correction term in the power spec- trum estimator that properly takes into account fiber collisions (Section 3.3).

3.2. First Method

Come up with better title for subsection

3.2.1. Line-of-Sight Displacement of Fiber Collided Pairs

It is impossible to determine definitely from observed galaxy data whether individual fiber collided galaxies without resolved spectroscopic redshift are correlated or chance alignments. Fortunately, using the fiber collided pairs with resolved redshifts (mainly in the overlapping

regions mentioned in Section 2), it is possible to model the line-of-sight displacement of the fiber collided pairs and measure the fraction of pairs that are correlated and uncorrelated.

For simulated mock catalogs, described in Section 2, modeling the fiber-collided galaxy pairs is a much more direct task since fiber collisions are post-processed after the simulated galaxy positions are generated. Redshift values are provided for all galaxies regardless of angular proximity and the fiber collisions imposed on the mock catalogs are represented through the galaxies' "fiber col- lision weights" ($w_{\rm fc}$). For example, in a situation where only two galaxies are within the fiber collision angular scale, the NN method assigns one galaxy ("the near- est neighbor") the fiber collision weight of both galax- ies ($w_{\rm fc} = 2$), while the other has $w_{\rm fc} = 0$. Nonetheless, since we actually have redshifts of both fiber-collided pair galaxies in mock catalogs, we can model the correlated and uncorrelated fiber-collided pairs in order to better understand the effects of fiber collisions.

To determine whether or not fiber collided pairs are correlated, we examine the comoving line-of-sight dis- placement ($d_{\rm LOS}$) of fiber collided galaxy pairs. We cal- culate the $d_{\rm LOS}$ by taking the difference of the line-of- sight comoving distance from the resolved redshifts:

$$d_{\rm LOS} = D_{\rm C}(z_1) - D_{\rm C}(z_2). \qquad (11)$$

$D_{\rm C}(z)$ is the line-of-sight comoving distance at redshift z (Hogg 1999). z_1 and z_2 represent the resolved redshifts of the two galaxies in the fiber collided pair.

After calculating the $d_{\rm LOS}$ for every fiber collided pairs, in Figure 4 we present the distribution of $d_{\rm LOS}$ for **LasDamas (blue), QPM (orange), Tiling Mock (green), and BOSS DR12 (black)**. All of the $d_{\rm LOS}$ distributions contain two components: a peak roughly contained within the range $-20\ {\rm Mpc} < d_{\rm LOS} < 20\ {\rm Mpc}$ and a flat component (hereafter "tail" component) out- side the peak that extends to $d_{\rm LOS} \sim \pm 500\ {\rm Mpc}$. The
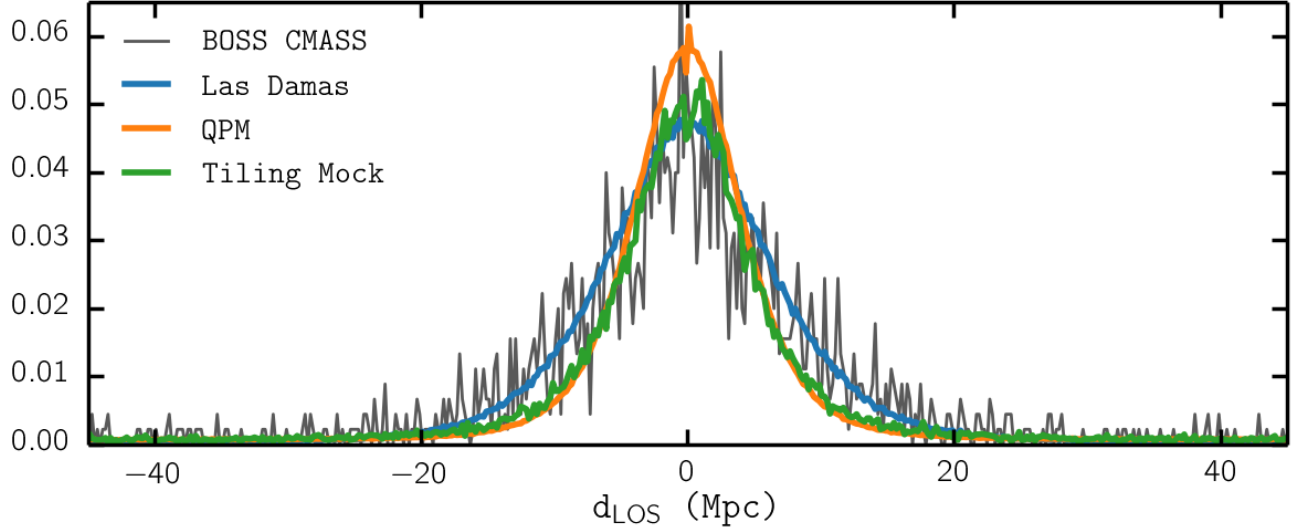
FIG. 4.— **bin CMASS with wider bins**Normalized distribution of d_{LOS} for LasDamas (blue), QPM (orange), and Tiling Mock (green) mock catalogs. The normalized d_{LOS} distribution of BOSS DR12 is also plotted (black). Bin size of $\Delta d = 0.2$ was used to compute the d_{LOS} distributions. The d_{LOS} distribution extends to $\sim \pm 500$ Mpc (not shown above). We focus on the peak of the distribution -20 Mpc $< d_{\mathrm{LOS}} < 20$ Mpc (discussed in 3.2.1).

entire range of the distribution is not displayed in Figure 4. For the BOSS data, since we cannot compute the d_{LOS} for fiber collided pairs without spectra, the d_{LOS} distribution only reflects the d_{LOS} from fiber collided pairs *with* resolved spectroscopic redshifts, mostly from tile overlapping regions of the BOSS survey.

Galaxies within the same halo, due to their gravitational interactions at halo-scales, are more likely to be in close angular proximity with each other. These galaxies in over-dense regions cause the peak in the d_{LOS} distribution. The "tail" component is composed of chance aligned galaxy pairs that happen to be in close angular proximity.

Focusing on the peak of the distribution, we note that it closely traces an Gaussian function. Therefore, we fit a Gaussian of the form,

$$p(d_{\mathrm{LOS}}) = A \, e^{-d_{\mathrm{LOS}}^2 / 2\sigma^2} \qquad (12)$$

for a mathematical prescription of the d_{LOS} distribution peak as a function of the displacement for each of the data catalogs in Figure 4. The best-fit σ and A parameters are obtained by fitting Equation 12 to the d_{LOS} distribution peaks using MPFIT (Markwardt 2009). We list the values of σ obtained for the mock catalogs in Table 1. Both Table 1 and Figure 4 illustrate that the d_{LOS} distributions for the mock catalogs closely trace the distribution of the BOSS DR12, which further goes to support the use of mock catalogs in our investigation.

Using the best-fit to the peak of the d_{LOS} distribution, we estimate the fraction of fiber collided pairs that are within the peak as

$$f_{\mathrm{peak}} = \frac{\sum\limits_{\mathrm{peak}} p(d_{\mathrm{LOS}})}{N_{\mathrm{pairs}}}, \qquad (13)$$

where N_{pairs} is the total number of fiber collided pairs. As mentioned above, this portion of fiber collided pairs are galaxy pairs that are correlated. We list the f_{peak}

TABLE 1
d_{LOS} DISTRIBUTION BEST-FIT PARAMETERS

catalog	σ (Mpc)	f_{peak}
LasDamas	6.85	0.71
QPM	4.98	0.65
Tiling Mock	5.38	0.57
BOSS DR12	7.6	0.65

Notes: **update this table** Best-fit parameter σ (Eq. 12) and peak fraction f_{peak} (Eq. 13) for the d_{LOS} distributions in Figure 4.

values for each of the data catalogs in Table 1. The f_{peak} values for the mock catalog are also in reasonable agreement with the BOSS DR12 f_{peak}.

For the NN method to be entirely correct, the d_{LOS} distribution in Figure 4 would have to be a delta function, which is clearly not the case. By simply incorporating the peak of the d_{LOS} distribution, we are able to significantly improve clustering statistics on small scales. Rather than placing the fiber collided galaxy on top of its nearest angular neighbor as the NN correction does, placing the fiber collided galaxy at a displacement, sampled from the d_{LOS} distribution, apart from its nearest neighbor better accounts for the small scale in clustering measurements.

On mock catalogs, we test this by first applying the NN to the mock catalogs. We then sample a displacement d_i from $p(d_{\mathrm{LOS}})$ (Equation 12) for each fiber collided pair. Afterwards we "place" the fiber collided galaxy a distance d_i from the nearest neighbor galaxy assign $w_{\mathrm{fc}} = 1$ and reduce the w_{fc} of the the nearest-neighbor by 1. We refer to this method as "d_{LOS}-peak".

Instead of describing dLOS peak only, describe how "peak-assigned" galaxies are determined.

Then transition to the shot noise correction term.
In Section 3.2.1 we derive a method to better statistically reconstruct the clustering of correlated fiber collided pairs using using the peak of the $d_{\rm LOS}$ distribution. Then in Section 3.3 we presented our formulation of the shot-noise correction term, which accounts for the added discreteness from chance aligned fiber collision pairs. We now combine these two methods and present our fiber collision correction method.

We begin once again with the fiber collided mock catalogs with the nearest-neighbor weights that accurately imitate the effects of fiber collision on the actual observed BOSS data. Then as described in Section 3.2.1, we calculate the $d_{\rm LOS}$ distribution of all fiber collided pairs in each mock catalog. From the $d_{\rm LOS}$ distribution, we compute the fraction of fiber collided pairs within the peak of the distribution ($f_{\rm peak}$; Section 3.2.1). We then select $f_{\rm peak}$ of the fiber collided pairs and designate them as correlated pairs that lie within the peak of the $d_{\rm LOS}$ distribution. We refer to these fiber collided pairs as "peak-assigned" pairs.

Each of these "peak-assigned" pairs, by the nearest-neighbor weights, consist of a galaxy with $w_{\rm fc} > 1$ (the "nearest-neighbor" galaxy) and another with $w_{\rm fc} = 0$ (the "collided" galaxy). We disregard the collided galaxy. For each of the nearest-neighbor galaxies, we sample a value $d_{\rm peak-assigned}$ from the Gaussian best-fit to the $d_{\rm LOS}$ distribution peak and place a galaxy with $w_{\rm fc} = 1$ at a comoving distance $d_{\rm peak-assigned}$ away from the nearest-neighbor galaxy. At the same time, we reduce $w_{\rm fc}$ of the nearest-neighbor galaxy (the one that was originally up-weighted) by 1. This process is repeated until the nearest-neighbor galaxy has $w_{\rm fc} = 1$ in the case of triplets or higher.

We keep the nearest-neighbor fiber collision weights imposed in the beginning for the remaining fiber collided pairs that are not "peak-assigned" ($1 - f_{\rm peak}$ of the fiber collided pairs). The resulting mock catalog has $f_{\rm peak}$ fewer galaxies with $w_{\rm cp} > 1$ compared to the fiber collided mock catalogs with nearest-neighbor weights that we started from; however, the total statistical weight ($\sum_{\rm gal} w_{\rm tot}$) of the mock catalog is conserved.

Next, we use the FKP estimator with the Eq. 20 shot-noise correction term described in Section 3.3 to calculate the $P(k)$ for our $d_{\rm LOS}$-peak corrected mock catalogs. In Figure 6, we present the ratio of the $\overline{P(k)}$ computed using our fiber collision correction method over $\overline{P_{\rm true}(k)}$. To assess the merit of the fiber collision correction, we once again over-plot the sample variance of the mock catalogs. For LasDamas, at $k \sim 0.3~h/{\rm Mpc}$, $P(k)/P_{\rm true}(k) - 1 \sim 0.5\%$ and throughout the k range, $0.3\% < P(k)/P_{\rm true}(k) - 1 < 1.3\%$. For QPM, at $k \sim 0.3~h/{\rm Mpc}$, $P(k)/P_{\rm true}(k) - 1 \sim 0.04\%$ and throughout the k range, $0.3\% < P(k)/P_{\rm true}(k) - 1 < 1.3\%$. **include numbers here when Ngrid=960 is done**. Moreover for the mock catalogs with sample variance measurements (LasDamas and QPM), the $P(k)$ ratio is significantly below the sample variance throughout the entire k range probed and even at $k \sim 0.3~h/{\rm Mpc}$.

3.3. *Shot Noise Correction*

Discuss the different shot-noise correction considerations in the literature Both the NN method and the $d_{\rm LOS}$-peak correction do not sufficiently account for the systematic effects of fiber collisions in the power spectrum. In this section we introduce the other part of our fiber collision correction method that involve the shot-noise correction term of the FKP power spectrum estimator. By modifying the shot noise term of the FKP estimator to account for fiber collisions, we present a more robust correction method that accounts for the chance aligned fiber collided pairs.

In Section 2, we described the FKP power spectrum estimator used to compute the power spectrums of Figure 2. In their estimator, to account for the discreteness of the density field, they subtract the shot-noise contribution to the power spectrum (Equation **??**):

$$P_{\rm shot} = \frac{(1+\alpha)\int d^3r~\bar{n}(\mathbf{r})w^2(\mathbf{r})}{\int d^3r~\bar{n}^2(\mathbf{r})w^2(\mathbf{r})}. \tag{14}$$

In practice, the integrals in Equation 14 can be written in terms of discrete sums over the random catalog. The spatial integral $\int d^3r~\bar{n}(\mathbf{r})...$ can be computed as the discrete sum $\alpha\sum_{\rm ran}....$ With this conversion,

$$P_{\rm shot}^{\rm FKP} = \frac{(1+\alpha)\alpha\sum_{\rm random} w_{\rm FKP}^2(\mathbf{r})}{\alpha\sum_{\rm random} w_{\rm FKP}^2(\mathbf{r})}. \tag{15}$$

However, in the FKP derivation, they do not take systematic weights of galaxies into account.

The spatial integral $\int d^3r~\bar{n}(\mathbf{r})...$ can also be computed using the mock catalogs rather than the synthetic random catalogs, as $\sum_{\rm gal} w_g...$ where w_g represents the statistical weight assigned to the galaxies (Cole et al. 2005; Yamamoto et al. 2006; Beutler et al. 2014; Gil-Marín et al. 2014). Then the shot-noise component can be expressed as:

$$P_{\rm shot} = \frac{\sum_{\rm galaxy} w_{\rm FKP}^2 w_g^2(\mathbf{r}) - \alpha^2\sum_{\rm random} w_{\rm FKP}^2(\mathbf{r})}{\alpha\sum_{\rm random} w_{\rm FKP}^2(\mathbf{r})}. \tag{16}$$

In this form, systematic weights for galaxies can be accounted for in the w_g and α terms.

Following the latter formulation, most recently, both Beutler et al. (2014) and Gil-Marín et al. (2014) formulate $P_{\rm shot}$ to account for systematic bias in their analysis of BOSS data. However, systematic weights are treated differently in each of their derivation. Keeping in mind the weights listed in Eq. 9 for the BOSS data, Beutler et al. (2014) derives

$$P_{\rm shot}^{\rm B2014} = \frac{\sum_{\rm galaxy} w_{\rm FKP}^2 w_{\rm tot}(\mathbf{r})w_{\rm sys}(\mathbf{r}) - \alpha'^2\sum_{\rm random} w_{\rm FKP}^2(\mathbf{r})}{\alpha'\sum_{\rm random} w_{\rm FKP}^2(\mathbf{r})}, \tag{17}$$

where $\alpha' = \sum_{\rm gal} w_{\rm tot}/N_{\rm ran}$.

On the other hand, Gil-Marín et al. (2014), in a formulation designed to account for fiber collisions derives $P_{\rm shot}$ using two separate components: one for correlated pairs and the other chance alignments. The shot-noise contribution to the power from correlated pairs (referred to as "true pairs" in Gil-Marín et al. 2014) is equivalent to Eq. 17 above ($P_{\rm shot}$ in Beutler et al. (2014)). For
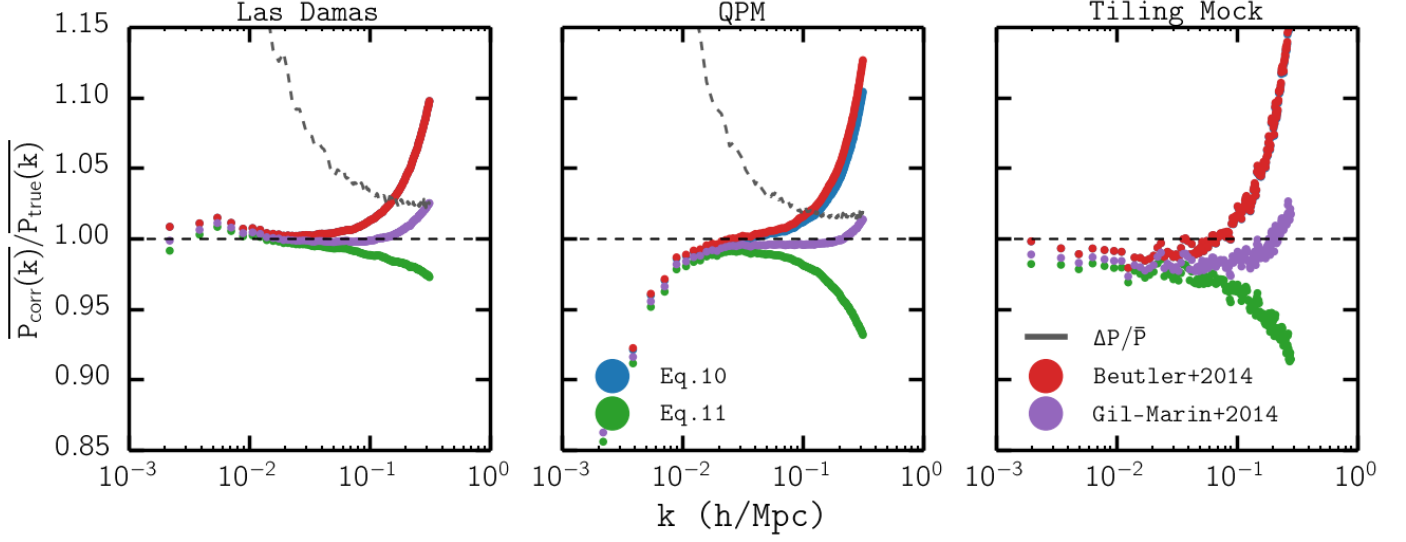
FIG. 5.— The ratio of $\overline{P_{\rm SN}(k)}$ computed using the shot-noise correction term given by Eq. 15 (blue), Eq. 20 (green), $P_{\rm shot}^{\rm B2014}$ (red), and $P_{\rm shot}^{\rm GM2014}$ (purple) over $\overline{P_{\rm true}(k)}$ for LasDamas (left panel), QPM (middle panel), and Tiling Mock (right panel) catalogs. We also plot $\Delta P_{\rm true}/P_{\rm true}(k)$ to compare with the sample variance ratio. $\overline{P_{\rm SN}(k)}$ computed using Eq. 15 shot-noise correction is identical to the NN method $\overline{P_{\rm corr}(k)}$ presented in Figure **??** and as before significantly overestimates $\overline{P_{\rm true}(k)}$ at $k > 0.1$ h/Mpc. $\overline{P_{\rm SN}(k)}$ using $P_{\rm shot}^{\rm B2014}$ equivalently overestimates $\overline{P_{\rm true}(k)}$ at $k > 0.1$ h/Mpc. On the other hand $\overline{P_{\rm SN}(k)}$ computed using Eq. 20 significantly underestimates the power spectrum at $k > 0.1$ h/Mpc with $\overline{P_{\rm SN}^{\rm Eq.15}}/\overline{P_{\rm true}}(k \sim 0.3) - 1 \sim -3\%, -8\%$, and -9 for LasDamas, QPM, and Tiling Mock respectively. $\overline{P_{\rm SN}(k)}$ computed using $P_{\rm shot}^{\rm GM2014}$ provides the best correction for fiber collisions ($\overline{P_{\rm SN}^{\rm GM2014}}/\overline{P_{\rm true}}(k \sim 0.3) - 1 \sim 2.5\%$). However at these small scales, even for $\overline{P_{\rm SN}^{\rm GM2014}}$ the effect of fiber collisions is comparable to sample variance at $k \sim 0.3$ h/Mpc.

chance alignments (referred to as "false pairs" in Gil-Marín et al. 2014), the shot-noise contribution is derived as,

$$P_{\rm shot}^{\rm False} = \frac{\sum\limits_{\rm galaxy} w_{\rm FKP}^2 w_{\rm tot}^2(\mathbf{r}) - \alpha'^2 \sum\limits_{\rm random} w_{\rm FKP}^2(\mathbf{r})}{\alpha' \sum\limits_{\rm random} w_{\rm FKP}^2(\mathbf{r})}. \quad (18)$$

Then the total $P_{\rm shot}$ is calculated as a combination of $P_{\rm shot}^{\rm True}$ and $P_{\rm shot}^{\rm False}$:

$$P_{\rm shot}^{\rm GM2014} = (1 - x_{\rm PS})P_{\rm shot}^{True} + x_{\rm PS}P_{\rm shot}^{False} \quad (19)$$

For analyzing BOSS $P(k)$ Gil-Marín et al. (2014) uses $x_{\rm PS} = 0.58$. The $x_{\rm PS}$ is calculated from the weighted galaxy catalog of Manera et al. (2013), not the observed BOSS data, and it is the value that optimizes the fit of the fiber collision corrected $P(k)$ to the $P_{\rm true}(k)$.

In our $P(k)$ calculations we use the FKP estimator with the shot-noise correction term computed as Eq. 16 with $w_{\rm g} = w_{\rm tot}$, which gives us,

$$P_{\rm shot}^{\rm Hahn+} = \frac{\sum\limits_{\rm galaxy} w_{\rm FKP}^2 w_{\rm tot}^2(\mathbf{r}) - \alpha'^2 \sum\limits_{\rm random} w_{\rm FKP}^2(\mathbf{r})}{\alpha' \sum\limits_{\rm random} w_{\rm FKP}^2(\mathbf{r})}. \quad (20)$$

We note that the difference between Eq. 20 and Eq. 17 lies in the first term of the numerator. In this term, for Eq. 17, $w_{\rm fc}$ is only included in $w_{\rm tot}$ and not in the $w_{\rm sys}$ term. However, Eq. 20 accounts for fiber collisions in the $w_{\rm tot}^2$ term. Also, Eq. 20 is equivalent to the shot-noise contribution from "false pairs" in Gil-Marín et al. (2014).

In order to compare the different $P_{\rm shot}$ derivations, we apply each of them ($P_{\rm shot}^{\rm FKP}$, $P_{\rm shot}^{\rm Hahn+}$, $P_{\rm shot}^{\rm B2014}$ and $P_{\rm shot}^{\rm GM2014}$) to the fiber collided mock catalogs with nearest-neighbor weights. To clarify, $P_{\rm shot}^{\rm FKP}$, $P_{\rm shot}^{\rm Hahn+}$, $P_{\rm shot}^{\rm B2014}$ and $P_{\rm shot}^{\rm GM2014}$ are calculated using Eq. 15, 20, 17 and 19, respectively. In our considerations of systematic effects beside fiber collisions in Eq. 9, we note that only the QPM mock catalog assigns $w_{\rm sys}$ (systematic weights due to sector completeness) to its galaxies and none of the mock catalogs assign $w_{\rm rf}$ to their galaxies. Therefore in Equations 9 - 15, for LasDamas and Tiling mock catalogs we use $w_{\rm sys} = w_{\rm rf} = 1$ so $w_{\rm tot} = w_{\rm fc}$ and for QPM mocks, we use $w_{\rm tot} = w_{\rm sys}w_{\rm fc}$. We compute the $P_{\rm SN}(k)$s using the FKP estimator with different $P_{\rm shot}$ prescriptions for each of the mock catalogs. We then average the power spectrum over the realizations to get $\overline{P_{\rm SN}(k)}$s for the mock catalogs, and then take the ratio over $\overline{P_{\rm true}(k)}$.

In Figure 5, we present $\overline{P_{\rm SN}(k)}/\overline{P_{\rm true}(k)}$ computed using $P_{\rm shot}^{\rm FKP}$, $P_{\rm shot}^{\rm Eq.20}$, $P_{\rm shot}^{\rm B2014}$ and $P_{\rm shot}^{\rm GM2014}$ shot noise correction term equations. $\overline{P_{\rm SN}(k)}$ calculated using $P_{\rm shot}^{\rm FKP}$ is the identical to the NN corrected $\overline{P(k)}$ in Figure **??**. Hence as before, it over estimates the $\overline{P_{\rm true}(k)}$ by $> 10\%$ for all mocks at $k \sim 0.3$ h/Mpc. $\overline{P(k)}$ measured using $P_{\rm shot}^{\rm B2014}$ (Eq. 17) does not significantly improve this overestimation in any of the mock catalogs. In fact for LasDamas and Tiling mock catalogs, since $w_{\rm sys} = 1$, $P_{\rm shot}^{\rm FKP} = P_{\rm shot}^{\rm B2014}$. Even for QPM, which assigns $w_{\rm sys}$ to its galaxies there are no significant improvements from using $P_{\rm shot}^{\rm B2014}$ over $P_{\rm shot}^{\rm FKP}$.

On the other hand, $\overline{P(k)}$ using Eq. 20 significantly is

significantly lower than the $\overline{P_{\text{true}}(k)}$. $\overline{P_{\text{SN}}^{\text{Eq.20}}}/\overline{P_{\text{true}}}(k \sim 0.3) - 1 \sim -3\%, -8\%,$ and -9 for LasDamas, QPM, and Tiling Mock respectively. Finally, $\overline{P(k)}$ measured using $P_{\text{shot}}^{\text{GM2014}}$ reproduces $\overline{P_{\text{true}}(k)}$ most accurately in the comparison of Figure 5. $\overline{P_{\text{SN}}^{\text{GM2014}}}/\overline{P_{\text{true}}}(k \sim 0.3) - 1 \sim 2.5\%$. As in Figure ??, we again plot the sample variance $(\Delta P/\bar{P})$ for each of the mock catalogs in Figure 5 for comparison. $\overline{P(k)}$ computed using $P_{\text{shot}}^{\text{Gil-Marin}}$ is able to best constrain the effects of fiber collisions in our comparison. However, even $\overline{P_{\text{SN}}^{\text{GM2014}}}$ is unable to significantly reduce the effects of fiber collisions below the sample variance, especially near $k \sim 0.3 \ h/\text{Mpc}$.

The shot-noise correction term we present in Eq. 20 should only correct for the shot-noise contribution to the power spectrum from chance alignment fiber collided pairs - not from correlated pairs. Because we apply the shot-noise correction to all fiber collided pairs indiscriminately in Figure 5, the shot-noise correction term oversubtracts the power spectrum as we find in Figure 5. In the following section we present our fiber collision correction method, that combines the d_{LOS}-peak correction of Section 3.2.1 and Eq. 20 from this section.

3.4. Second Method

??

- **Figure of 2PCF that demonstrates a pretty clear tophat**

- **The ultimate equations for calculating the tophat convolution**

- **Polynomials estimations of the integral?**

- **Figures of the fourier tophat method in action**

4. RESULTS

4.1. Goodness-of-fit

The correction method we present in this paper corrects for the effect of fiber collisions to the extent where $P_{\text{corr}}(k)$ measurements are no longer dominated by systematic effects at the scales probed in our calculations, even for the smallest scales of $k \sim 0.3 \ h/\text{Mpc}$. However, to further quantify how accurately our correction method is able to reproduce the true power spectrum and correct for the effects of fiber collisions, we quantify the goodness-of-fit for all the corrected $P(k)$s to $P_{\text{true}}(k)$ by calculating the following χ^2:

$$\chi^2(k_{\max}) = \frac{1}{N_{k_{\max}}} \sum_{k < k_{\max}} \frac{(\overline{P_{\text{corr}}(k)} - \overline{P_{\text{true}}(k)})^2}{\Delta P_{\text{true}}(k)^2}. \quad (21)$$

$N_{k_{\max}}$ is the number of k bins in the $P(k)$ calculation with $k < k_{\max}$. $\overline{P_{\text{corr}}(k)}$ is the average fiber collision corrected powerspectrum of all realizations for each catalog. $\Delta P_{\text{true}}(k)$ is the standard deviation of $P_{\text{true}}(k)$ computed from all realizations of each mock catalog. We calculate χ^2 as a function of $k_{\max}$ in order to determine the accumulated χ^2 to a specific scale $(k_{\max})$. In doing so, we determine the scale to which a power spectrum analysis

can be extended to without fiber collisions dominating the measurement.

For the Tiling Mock catalog, since there is only one realization, the variance $(\Delta P_{\text{true}}(k))$ cannot be computed independently. However, for an estimate of the χ^2, we estimate $\Delta P_{\text{true}}^{\text{Tiling Mock}}(k)$ from $\Delta P_{\text{true}}^{\text{QPM}}(k)$ scaled by the ratio of the power spectrums:

$$\Delta P_{\text{true}}^{\text{Tiling}}(k) = \Delta P_{\text{true}}^{\text{QPM}}(k) \times \frac{P_{\text{true}}^{\text{Tiling}}(k)}{P_{\text{true}}^{\text{QPM}}(k)}. \quad (22)$$

In Figure 7, we present the $\chi^2(k_{\max})$ for $P(k)$ using the following fiber collision correction methods: the NN correction (also Anderson et al. 2012), Beutler et al. (2014), Gil-Marín et al. (2014), and our method from Section **??**. The comparison is made using the LasDamas (left panel), QPM (center panel) and Tiling (right panel) mock catalogs. First in the LasDamas panel, at scales larger than $k_{\max} < 5 \times 10^{-2} \ h/\text{Mpc}$, $\chi^2 < 10^{-3}$ for all correction methods, which suggests that all correction methods sufficiently correct for fiber collisions and reasonably reconstructs $P_{\text{true}}(k)$ at these scale. In approaching smaller scales the χ^2 for all correction methods increase. However, throughout the entire $k_{\max}$ range, our correction method provides a notably lower χ^2 in comparison to the other correction methods. This is especially clear at $k_{\max} \sim 0.3 \ h/\text{Mpc}$, where $\chi^2_{\text{NN}} \approx 0.33$, $\chi^2_{\text{B2014}} \approx 0.33$, and $\chi^2_{\text{GM2014}} \approx 0.17$ while $\chi^2 \approx 0.019$ for our method.

Next in the QPM panel (center), at scales larger than $k_{\max} < 2 \times 10^{-2} \ h/\text{Mpc}$ all corrected $P(k)$ again provide a reasonable reconstruction of $P_{\text{true}}(k)$ with $\chi^2 \approx 10^{-2}$. Then for $2 \times 10^{-2} < k_{\max} < 5 \times 10^{-2} \ h/\text{Mpc}$, the NN and Beutler et al. (2014) correction methods have the lower χ^2s than Gil-Marín et al. (2014) and our correction methods. However, as $k_{\max}$ increases, the χ^2s for NN and Beutler et al. (2014) quickly surpasses the χ^2s of Gil-Marín et al. (2014) and our method. Meanwhile, throughout the entire $k_{\max}$ range probed, our correction method has a significantly lower χ^2 than the correction method of Gil-Marín et al. (2014). The difference in χ^2 is again most remarkable at the smallest scales: $\chi^2(k_{\max} \sim 0.3) \approx 7.3$, 11, 0.068, and 0.0063 for NN, Beutler et al. (2014), Gil-Marín et al. (2014) and our correction method respectively.

Finally for the Tiling mock catalog (right panel), we find that $\chi^2(k_{\max})$ increases in a near monotonic fashion as a function of $k_{\max}$. For $k_{\max} < 4 \times 10^{-2} \ h/\text{Mpc}$, there are no significant differences between the χ^2s of any of the correction methods. Then at intermediate scales of $4 \times 10^{-2} < k_{\max} < 1.5 \times 10^{-2} \ h/\text{Mpc}$, χ^2s of NN and Beutler et al. (2014) are notably lower than the χ^2s of Gil-Marín et al. (2014) and our method. However like the other mock catalogs at smaller scales, the χ^2s of NN and Beutler et al. (2014) quickly increase beyond the other χ^2s, ultimately both reach $\chi^2(k_{\max} \sim 0.3) \approx 13.5$. In the meantime, $\chi^2(k_{\max} \sim 0.3) \approx 0.32$ for Gil-Marín et al. (2014) and $\chi^2(k_{\max} \sim 0.3) \approx 0.15$ for our correction method. Throughout the entire $k_{\max}$ our method has a lower χ^2 than Gil-Marín et al. (2014). With only one realization of the Tiling mock catalog and scaled ΔP, a detailed comparison of the χ^2 values is difficult. Yet
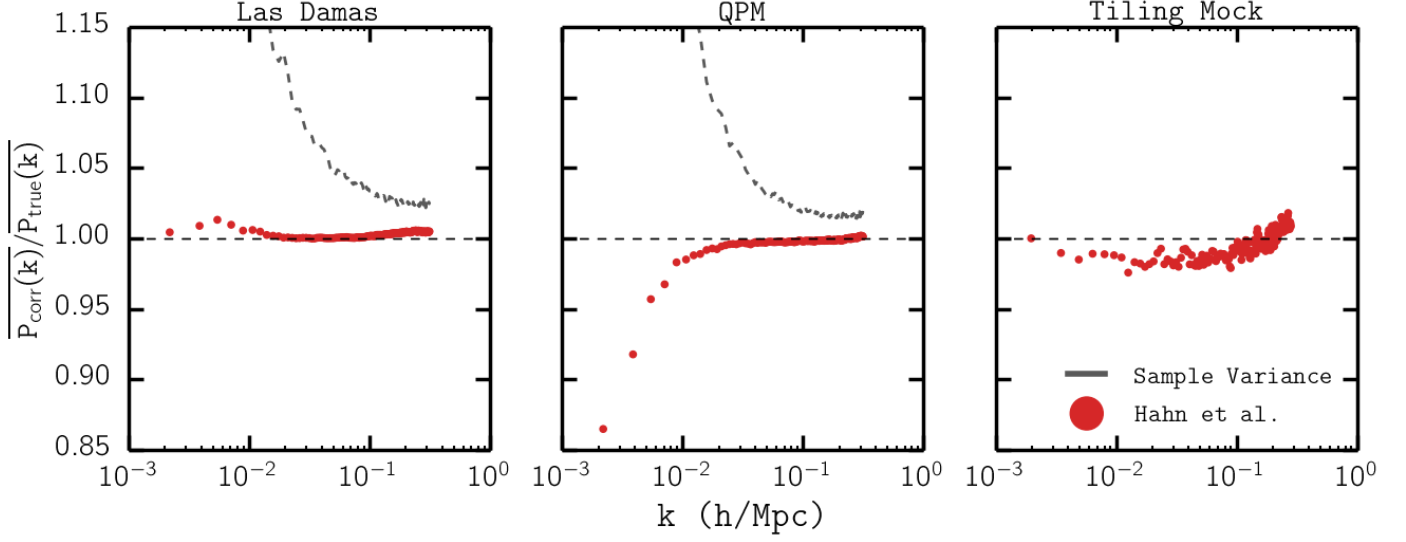
FIG. 6.— The ratio of $\overline{P(k)}$ computed using our fiber collision correction method presented in Section **??** over $\overline{P_{\text{true}}(k)}$ for LasDamas (left panel), QPM (middle panel), and Tiling Mock (right panel) catalogs with nearest-neighbor fiber collision weights (red). We again plot $\Delta P_{\text{true}}/P_{\text{true}}(k)$ for comparison. $\overline{P_{\text{corr}}}/\overline{P_{\text{true}}}(k \sim 0.3\ h/\text{Mpc}) - 1 \sim 0.5\%$ for our fiber collision correction. This is significantly better than the correction methods of Anderson et al. (2012), Beutler et al. (2014) and Gil-Marín et al. (2014) in Figure 5. Moreover, for LasDamas and QPM, our correction method is able to correct for the effects of fiber collisions, significantly below the $\Delta P_{\text{true}}/P_{\text{true}}(k)$ throughout the probed k range, even at the smallest scales.
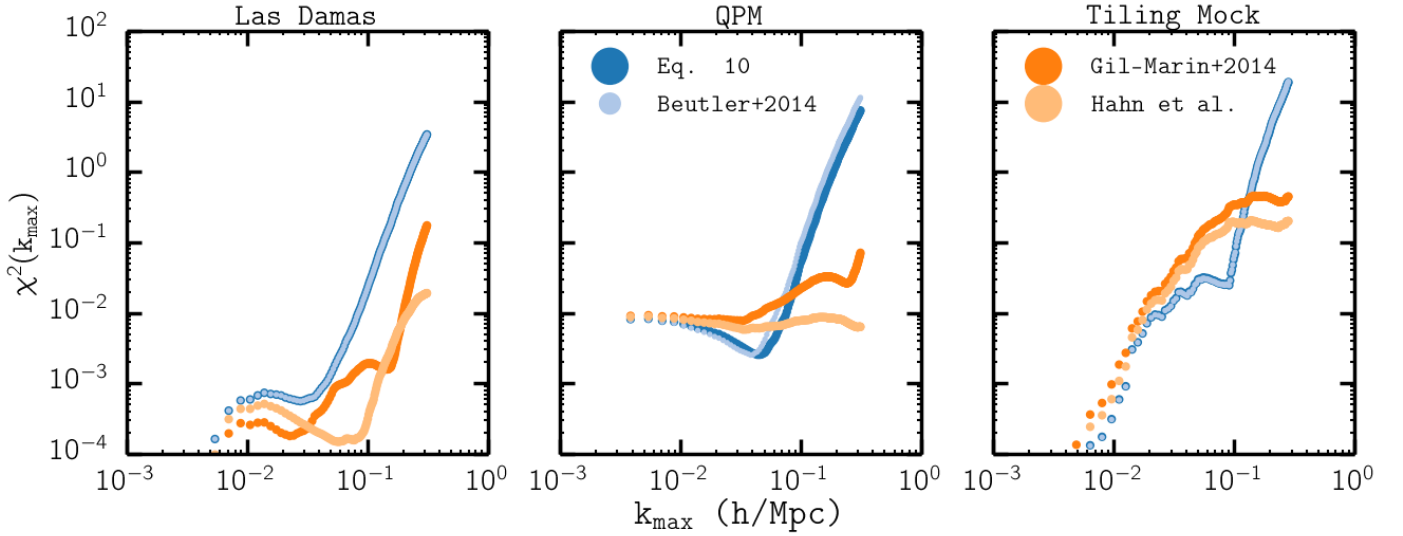

FIG. 7.— $\chi^2(k_{\text{max}})$ for $P_{\text{NN−upweight}}$ (blue), P_{Beutler} (light blue), $P_{\text{Gil−Marin}}$ (orange), and P_{Hahn} (yellow) using the LasDamas (left panel), QPM (centerl panel), and Tiling (right panel) mock catalogs. Equation 21 was used to compute the $\chi^2(k_{\text{max}})$.

the $\chi^2(k_{\text{max}})$ results for our correction provide realistic assurance that the correction method can be applied to the actually BOSS data.

Overall, regardless of catalog, for scales $k_{\text{max}} < 3 \times 10^{-2}\ h/\text{Mpc}$, the χ^2 for all fiber collision corrected $P(k)$ are negligible. Then, with the exception of the Las-Damas catalog, at intermediate scales of $3 \times 10^{-2} < k_{\text{max}} < 0.15\ h/\text{Mpc}$ the NN and Beutler et al. (2014) methods show the lowest χ^2s. However at these intermediate scales, all of the correction methods reasonably reconstruction of the true power spectrum with $\chi^2 \ll 1$. At the smallest scales, NN and Beutler et al. (2014) corrections methods no longer provide a sufficient fit

to $\overline{P_{\text{true}}(k)}$. A detailed comparison at the small scales ($k > 1.5 \times 10^{-1}\ h/\text{Mpc}$) demonstrates that the fiber collision correction we present in this paper significantly better reproduces the true power spectrum than any of the other fiber collision correction methods. Furthermore, Figure 7 illustrates that throughout the entire k_{max}, our correction method is able to reasonably reproduce $P_{\text{true}}(k)$ at all scales.

5. SUMMARY AND DISCUSSION

Using simulated mock catalogs for SDSS data with realistically imposed fiber collisions, we quantify the systematic effects of fiber collisions on galaxy clustering

measurements - in particular the power spectrum. Although fiber collisions have little significant effect on the power spectrum at large scales, their effect quickly overtakes the sample variance at scales smaller than $k > 0.1 \ h/\mathrm{Mpc}$. At the smallest scales that we explore in this paper, $k \sim 0.3 \ h/\mathrm{Mpc}$, fiber collisions have over a 10% effect on the power spectrum. Consequently at these small scales, measurements of the power spectrum is dominated by the uncertainties from systematic effects of fiber collisions.

Fortunately, using the fiber collided mock catalogs used in this paper, we are able to model the distribution of the line-of-sight displacement between fiber collided pairs. With this model, we are able to statistically reconstruct the clustering fiber collided galaxies that reside in the same halo. Combining this correction with a modification of the shot-noise term in the power spectrum estimator to properly account for the discreteness added by the nearest-neighbor weights of chance aligned fiber collided pairs, we devise a new fiber collision correction method that is able to reconstruct the true power spectrum from fiber collided data even to $k \sim 0.3 \ h/\mathrm{Mpc}$. Throughout the entire k range explored in our analysis, our correction method reconstructs $P_{\mathrm{true}}(k)$ safely within the sample variance.

Furthermore, we compare our method to the most common nearest-neighbor correction method (Zehavi et al. 2002; Berlind et al. 2006; Anderson et al. 2012) and recent correction methods presented in Beutler et al. (2014) and Gil-Marín et al. (2014) to demonstrate that our method most successfully reproduces the true power spectrum at small scales and most reliably at all scales for all the LasDamas, QPM, and Tiling mock catalogs. Furthermore, while the correction method of Gil-Marín et al. (2014) is comparable our correction method, the parameter x_{PS} used in the method is calculated solely through a weighted galaxy mock catalog. As an added advantage, our correction method can also be callibrated by the observed data rather than only through the mock catalogs. Therefore our correction method does not depend on the accuracy of the mock catalogs, thereby making it's application to observations further reliable.

The fiber collision correction method we present will enable us to extend our galaxy clustering analysis to smaller scales for SDSS-III BOSS and future surveys such as eBOSS or any other large fiber-fed surveys the suffer from systematic effects of fiber collisions. Our fiber collision correction method can also be extend to higher order clustering statistics such as the quadrupole of the power spectrum and the bispectrum, which we will explore in future work.

REFERENCES

Anderson, L., Aubourg, E., Bailey, S., et al. 2012, MNRAS, 427, 3435

Berlind, A. A., Frieman, J., Weinberg, D. H., et al. 2006, ApJS, 167, 1

Beutler, F., Saito, S., Seo, H.-J., et al. 2014, MNRAS, 443, 1065

Cole, S., Percival, W. J., Peacock, J. A., et al. 2005, MNRAS, 362, 505

Colless, M. 1999, Royal Society of London Philosophical Transactions Series A, 357, 105

Davis, M., Efstathiou, G., Frenk, C. S., & White, S. D. M. 1985, ApJ, 292, 371

Dawson, K. S., Schlegel, D. J., Ahn, C. P., et al. 2013, AJ, 145, 10

Dawson, K. S., Kneib, J.-P., Percival, W. J., et al. 2015, ArXiv e-prints, arXiv:1508.04473

Feldman, H. A., Kaiser, N., & Peacock, J. A. 1994, ApJ, 426, 23

Gil-Marín, H., Noreña, J., Verde, L., et al. 2014, ArXiv e-prints, arXiv:1407.5668

Guo, H., Zehavi, I., & Zheng, Z. 2012, ApJ, 756, 127

Heitmann, K., Lukić, Z., Fasel, P., et al. 2008, Computational Science and Discovery, 1, 015003

Hogg, D. W. 1999, ArXiv Astrophysics e-prints, astro-ph/9905116

Makarem, L., Kneib, J.-P., Gillet, D., et al. 2014, A&A, 566, A84

Manera, M., Scoccimarro, R., Percival, W. J., et al. 2013, MNRAS, 428, 1036

Markwardt, C. B. 2009, in Astronomical Society of the Pacific Conference Series, Vol. 411, Astronomical Data Analysis Software and Systems XVIII, ed. D. A. Bohlender, D. Durand, & P. Dowler, 251

McBride, C., Berlind, A., Scoccimarro, R., et al. 2009, in Bulletin of the American Astronomical Society, Vol. 41, American Astronomical Society Meeting Abstracts #213, 425.06

McBride, C., Berlind, A. A., Scoccimarro, R., et al. 2011, in Bulletin of the American Astronomical Society, Vol. 43, American Astronomical Society Meeting Abstracts #217, 249.07

Morales, I., Montero-Dorta, A. D., Azzaro, M., et al. 2012, MNRAS, 419, 1187

Schlegel, D., Abdalla, F., Abraham, T., et al. 2011, ArXiv e-prints, arXiv:1106.1706

Schneider, A., Teyssier, R., Potter, D., et al. 2015, ArXiv e-prints, arXiv:1503.05920

Scoccimarro, R. 2015, Phys. Rev. D, 92, 083532

Scoccimarro, R., & Sheth, R. K. 2002, MNRAS, 329, 629

Tinker, J. L., Sheldon, E. S., Wechsler, R. H., et al. 2012, ApJ, 745, 16

White, M., Tinker, J. L., & McBride, C. K. 2014, MNRAS, 437, 2594

Yamamoto, K., Nakamichi, M., Kamino, A., Bassett, B. A., & Nishioka, H. 2006, PASJ, 58, 93

Yoon, J. H., Schawinski, K., Sheen, Y.-K., Ree, C. H., & Yi, S. K. 2008, ApJS, 176, 414

Zehavi, I., Blanton, M. R., Frieman, J. A., et al. 2002, ApJ, 571, 172

Zehavi, I., Zheng, Z., Weinberg, D. H., et al. 2005, ApJ, 630, 1